Complex periodic orbits in the rotational spectrum of molecules: The example of SF_6

Jonathan M. Robbins, Stephen C. Creagh, and Robert G. Littlejohn
Department of Physics, University of California, Berkeley, California 94720
(Received 26 July 1988; revised manuscript received 15 November 1988)

Periodic orbit theory expresses, in a semiclassically approximate way, the trace of the energy-dependent Green's function of a quantum-mechanical system in terms of a sum over periodic orbits of the corresponding classical system. In this paper a periodic orbit sum is carried out for a Hamiltonian describing the rotational dynamics of the SF_6 molecule. Following Miller [J. Phys. Chem. **83**, 960 (1979)], classically forbidden, or "tunneling" orbits are included in the sum. A closed-form expression for the trace of the energy-dependent Green's function is obtained; it depends on the actions and Maslov indices of the classical orbits, as well as the irreducible representatives of the generators of the molecular point group. The expression reproduces the rich structure characteristic of the rotational spectra of symmetric molecules, including the exponentially near degeneracies for large angular momentum, and the periodicities in eigenvalue symmetry assignments. The methods used here complement the extensive studies of Harter and Patterson.

I. INTRODUCTION

Periodic orbit theory, developed by Gutzwiller,[1] Balian and Bloch,[2] and Berry,[3] provides a semiclassical determination of the spectra of quantum-mechanical systems. The theory relates the trace of the energy-dependent Green's function (alternatively, the quantum-mechanical density of states) to a sum over classical periodic orbits. Applications have included the anisotropic Kepler problem,[4] force-free motion on a surface of constant negative curvature,[5] and most recently, the hydrogen atom in a strong magnetic field,[6,7] a system for which the predictions of the theory can be compared directly with experiment.

In its present form, periodic orbit theory applies to systems whose classical dynamics is chaotic. Indeed, it provides the only known analytical results concerning such systems, and is an important tool in the study of quantum chaos. In this paper we pursue a rather different application of periodic orbit theory, namely, the calculation of quantum tunneling effects. The novel idea is to include complex, or classically forbidden orbits as well as real, or classically allowed orbits in the periodic orbit sum. Our approach follows Miller's work on the double well oscillator;[8] several other authors have investigated the role of complex orbits in periodic orbit theory.[9–12] A principal advantage of all these treatments is their representation independence. Periodic orbit theory involves only geometrical and topological features of the classical dynamics, and its formulation is coordinate free. Traditional treatments of tunneling are usually committed to a particular representation, which obscures the underlying phase-space structure of the semiclassical approximation.

Tunneling effects play an essential role in the rotational spectra of symmetric molecules, such as SF_6. Ultrahigh-resolution spectroscopy has revealed a rich and complex structure in the rotational spectrum of SF_6.[13–18] Vibration-rotation interactions destroy the spherical symmetry of the molecular moment of inertia tensor, introducing fine structure into the rotational spectrum. Tunneling between equivalent rotational motions produces a superfine structure within the fine structure. There also appears a remarkable periodicity in the eigenvalue symmetry assignments which cannot be explained on the basis of standard group theory. The theory underlying these spectra has been extensively developed,[19–21] most notably by Harter and Patterson.[22–25] Their elegant treatment combines semiclassical ideas and results from the theory of induced representations within the framework of degenerate perturbation theory.

Notwithstanding its success and intuitive appeal, the semiclassical treatment of Harter and Patterson is heuristic in nature. Also, it is not fully semiclassical, in that it involves a quantum-mechanical calculation with semiclassical input. A systematic semiclassical analysis along the lines of traditional WKB theory is difficult to carry out because the rotational Hamiltonian is not simply a sum of kinetic and potential terms. In this paper we apply periodic orbit theory to the SF_6 rotational Hamiltonian, and include both real and complex classical trajectories in the analysis. We obtain results equivalent to those of Harter and Patterson, including the periodicity in symmetry assignments. Our approach is fully semiclassical, and involves no quantum-mechanical manipulations, such as matrix diagonalization.

The paper is organized as follows. In Sec. II we formulate the complex periodic orbit sum, and carry out the sum for the symmetric double well. The example serves as a pattern for the more complicated SF_6 calculation to follow. In Sec. III we present a model for the SF_6 rotational dynamics. We discuss the classical version of the model, upon which the complex periodic orbit sum is based, as well as the quantum version, from which the fine and superfine structures emerge. In Sec. IV we carry out the complex periodic orbit sum for the SF_6 model Hamiltonian. Section V concludes with a summary of the results and a discussion of questions for further investigation.

II. COMPLEX PERIODIC ORBIT SUM

Periodic orbit theory establishes a semiclassically approximate relationship between the spectrum of a quantum-mechanical system and the periodic orbits of its corresponding classical system. The case of one degree of freedom is a special one. Systems of one degree of freedom are not chaotic, and yet periodic orbit theory can be applied to them. One obtains the following semiclassical formula for the trace of the energy-dependent Green's function $g(E)$:[26]

$$g_{\rm sc}(E)=\frac{1}{i\hbar}\sum_j T_j \sum_{k=1}^{\infty} e^{ik(S_j/\hbar-\mu_j\pi/2)} , \tag{2.1}$$

where the notation "sc" means "semiclassical." The right-hand side of Eq. (2.1) is a sum over classical periodic orbits with energy E. The index j labels the primitive periodic orbits. (A primitive periodic orbit is a single traversal of a periodic orbit.) For simple Hamiltonians of the form $T+V$, with single well potentials, there is only one such orbit. But for multiple well potentials and for more general Hamiltonians, there may be many. T_j is the period of the jth orbit, and S_j is the action integral, $\oint p\,dq$ taken around it. μ_j is the Maslov index of the jth orbit. The sum over k effectively includes multiple traversals of the jth orbit in the sum.

For bound systems, the energy levels of the Hamiltonian $\hat{H}$ can be completely determined from $g(E)$. (Throughout this paper, a caret is used to distinguish quantum operators from their classical counterparts.) From the definition $g(E)=\mathrm{Tr}[(E-\hat{H})^{-1}]$, we obtain

$$g(E)=\sum_n \frac{d_n}{E-E_n} . \tag{2.2}$$

The poles of $g(E)$ are the eigenvalues E_n of $\hat{H}$, and the pole strengths are the eigenvalue degeneracies d_n. Together, Eqs. (2.1) and (2.2) provide a semiclassical determination of the spectrum of systems of one degree of freedom. Indeed, the summations of Eq. (2.1) can be carried out explicitly. The result yields the Einstein-Brillouin-Keller (EBK) quantization rule[13] for one degree of freedom systems.

It is well known that quantum-mechanical tunneling introduces corrections to the EBK rule, and there exists an extensive literature devoted to tunneling in one dimension.[26,27] Several authors have used periodic orbit theory to treat tunneling effects.[8–12] These treatments possess an important property not found in traditional treatments, namely, representation independence. Equation (2.1) serves as an illustration of what we mean by representation independence. It relates a quantum expression to a classical expression. The classical expression is clearly independent of any particular choice of canonical coordinates; it involves periods, actions, and Maslov indices, all of which are geometrical or topological properties of the periodic orbits. The quantum side of the equation is clearly independent of any particular choice of representation; it involves the trace of an operator. For both theoretical and practical reasons, representation independence is a desirable feature of any semiclassical theory.

Our calculation of tunneling effects in the SF_6 rotational spectrum follows the work of Miller.[8] Miller introduced tunneling trajectories into the periodic orbit sum and obtained the tunneling splittings in the energy levels of the double well oscillator. The rest of this section is organized as follows. In Sec. II A we present a prescription, Eq. (2.3) below, for the complex periodic orbit sum. The prescription is similar to Miller's, although it includes a larger family of complex periodic orbits. It is particularly suited to systems which have a discrete symmetry. As a simple application of Eq. (2.3), in Sec. II B we carry out the complex periodic orbit sum for the symmetric double well oscillator, for which the symmetry is parity. Some modifications of Miller's original calculation are discussed.

A. Prescription

The complex periodic orbit sum is obtained by including complex, or classically forbidden orbits, as well as real, or classically allowed orbits, in the sum of Eq. (2.1). We shall regard this prescription as heuristic, and shall not attempt a derivation here. More rigorous treatments may be found in the references.[9,10]

We restrict our attention to a system of one degree of freedom with a discrete symmetry, and assume that its primitive periodic orbits are related by this symmetry. (Throughout this discussion, a primitive periodic orbit is understood to be real.) The complex periodic orbit sum is given by

$$g_{\rm sc}(E)=\frac{f}{i\hbar}T\sum_k e^{i(\Gamma_k/\hbar-\mu_k\pi/2)} . \tag{2.3}$$

Here, f is the number of primitive periodic orbits with energy E. Note that f may depend on the energy. For example, for the double well, there are two primitive periodic orbits at energies below the barrier, and one orbit at energies above. The period of the primitive periodic orbits is T. The index k labels the complex periodic orbits with energy E. (As a matter of terminology, we consider the real periodic orbits to be a subset of the complex periodic orbits.) Γ_k is the action, $\oint p\,dq$ of the kth orbit, and μ_k is its Maslov index. Note that Γ_k may be complex.

To complete this explanation of the complex periodic orbit sum, we must discuss the complex periodic orbits themselves. What are they, and which ones are to be included in the sum? There are several ways to define complex periodic orbits; the following, appropriate to systems of one degree of freedom, is well suited to our discussion. A real periodic orbit may be thought of as a closed curve on the real energy shell. We take a complex periodic orbit to be a closed curve on the complex energy shell.

The real energy shell is one dimensional (indeed, it is composed of the primitive periodic orbits), and it contains a countable set of periodic orbits, which correspond to multiple traversals of the primitive periodic orbits. The complex energy shell, on the other hand, is two dimensional, and contains a continuum of closed curves, or

periodic orbits. In order to make sense of the sum over complex periodic orbits, we must designate a countable subset of this continuum. In what follows, we give several rules to determine the subset of orbits to be included in the complex periodic orbit sum.

First, we include only complex periodic orbits which begin and end at some fixed point on a (real) primitive periodic orbit. We shall call this point the *base point.* The complex periodic orbit sum does not depend on which of the primitive periodic orbits the base point is chosen to lie upon, as these orbits are all related by symmetry. A typical orbit in the sum begins at the base point, wanders about the complex energy shell, perhaps visiting other primitive periodic orbits before returning to the base point.

The second rule is that we include only *topologically distinct* orbits in the sum. Two orbits are said to be *topologically equivalent* if one can be continuously deformed into the other while keeping the orbit confined to the complex energy shell and its endpoints fixed at the base point. Singularities on the complex energy shell may prevent such a deformation from being realized, in which case we say that the orbits are topologically distinct. As defined above, topological equivalence is an equivalence relation in the mathematical sense. Therefore, the complex periodic orbits may be divided into classes of topologically equivalent orbits. Restated, the second rule requires that we include in the sum at most one orbit from each class of equivalent orbits. It is this rule which limits the sum to a countable set of orbits.

An important fact about topologically equivalent orbits is that they have the same actions and the same Maslov indices. As a result, the complex periodic orbit sum does not depend on which orbits are chosen to represent the classes. We will take advantage of this fact, and choose as representatives orbits which possess certain properties. These *special representative orbits,* as we shall call them, consist of segments along which the action differential, $p\,dq$ is either purely real or purely imaginary. Segments with real action are called *classical segments;* they are segments of the primitive periodic orbits. Segments along which the action differential is imaginary are called tunneling segments. A useful feature of the special representative orbits is that they are easily parametrized in terms of sequences of classical and tunneling segments.

The third and fourth rules are most easily stated in terms of the special representative orbits, and concern the sense in which the classical and tunneling segments are to be traversed. According to the third rule, a class of equivalent orbits is included in the sum only if it contains a special representative orbit whose action $\int p\,dq$ along each of its tunneling segments is positive imaginary. This means that the contributions of the tunneling segments to the complex periodic orbit sum must be exponentially damped, rather than exponentially enhanced. The fourth rule determines the sense of traversal of the classical segments. A class is included in the sum only if it contains a special representative orbit which traverses each of its classical segments in the sense determined by Hamilton's equations. In other words, along classical segments the orbit must move forward in real time. Note that the orbits in the real periodic orbit sum, Eq. (2.1) also move forward in time.

Let us summarize. A complex periodic orbit is a closed curve on the complex energy shell. The complex periodic orbit sum of Eq. (2.3) is taken over topologically distinct, complex periodic orbits beginning and ending at the base point, which lies on a real periodic orbit. For convenience, we sum over special representative orbits composed of classical and tunneling segments. To be included in the sum, a special representative orbit must have positive imaginary action along each tunneling segment, and must move forward in real time along each classical segment.

B. An example: The symmetric double well

In this section we carry out the complex periodic orbit sum for the symmetric double well potential. Throughout the calculation, we set $\hbar=1$. We consider energies E below the barrier (the calculation is easily modified to treat energies above). We take the base point of the complex periodic orbits to be the turning point A, indicated in Fig. 1. The classical and tunneling segments are also shown in Fig. 1. The classical segments coincide with the primitive periodic orbits in each of the two potential wells. The two tunneling segments are paths joining the turning points A and B, along which the momentum p is either positive or negative imaginary. As discussed in Sec. II A, we consider special representative orbits composed of classical and tunneling segments. Such orbits oscillate in, and tunnel back and forth between the two potential wells. Along classical segments, the orbits must move forward in real time. On tunneling from A to B, the orbits must take the tunneling segment with positive imaginary momentum, while on tunneling from B to A, the tunneling segment with negative imaginary momentum.

The main difficulty in carrying out the sum is the parametrization of the complex periodic orbitals. We must make sure that all of the orbits which should be included are included, and that each of these orbits is counted only once. Let us call a sequence of consecutive classical segments a *classical episode,* and a sequence of consecutive tunneling segments a *tunneling episode.* It is clear that the special representative orbits consist of an alternating

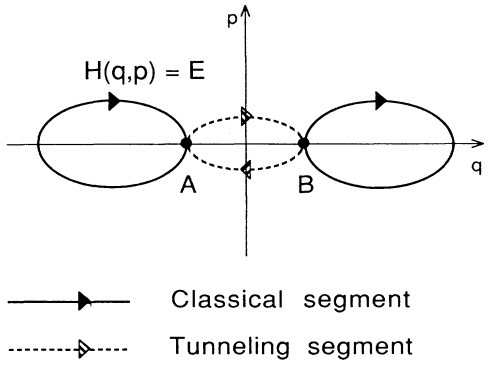

FIG. 1. Complex energy shell for the symmetric double well.

sequence of classical and tunneling episodes. We can parametrize the orbits by a sequence of integers which describe both the number and the duration of these episodes, as follows:

$$\{n;a_0,b_1,\ldots,a_n,b_{n+1}\}\ ,$$
$$n=0,1,2,\ldots$$
$$a_0=0,1,2,\ldots$$
$$a_1,\ldots,a_n,b_1,\ldots,b_n=1,2,\ldots$$
$$b_{n+1}=0,1,2,\ldots\ . \tag{2.4}$$

Here, $n+1$ gives the number of classical and tunneling episodes in the orbit, a_k is the number of classical segments in the kth classical episode, and b_k is the number of tunneling segments in the kth tunneling episode. Thus, the sequence $\{n;a_0,b_1,\ldots,a_n,b_{n+1}\}$ describes an orbit which consists of a_0 classical segments, followed by b_1 tunneling segments , . . . , followed by a_n classical segments, followed by b_{n+1} tunneling segments.

The parameter ranges insure that all orbits are included in the parametrization, and that the parametrization is unique. Since $n+1$ determines the number of distinct classical and tunneling episodes, each of these episodes must contain at least one segment. That is, we require that $a_k \geq 1$ and $b_k \geq 1$. There are two exceptions to this rule. We allow a_0 to be zero to account for trajectories which begin with a tunneling episode. Similarly, we allow b_{n+1} to be zero to account for trajectories which end with a classical episode.

Having parametrized the complex periodic orbits, we compute their actions and Maslov indices. Let S be the action, $\oint p\,dq$ taken around either of the primitive periodic orbits. Let $i\theta$ be the imaginary action computed along one of the tunneling segments between A and B such that θ is positive. Then the action of the orbit $\{n;a_0,b_1,\ldots,a_n,b_{n+1}\}$ is given by

$$\Gamma\{n;a_0,b_1,\ldots,a_n,b_{n+1}\}=S\sum_{k=0}^{n}a_k+i\theta\sum_{k=1}^{n+1}b_k\ . \tag{2.5}$$

Next, we determine the Maslov indices. The primitive periodic orbits have two turning points, so we increment the Maslov index by 2 for each classical segment. However, the Maslov index should not be incremented when an orbit tunnels through a turning point, i.e., when a tunneling segment follows a classical segment. To compensate, we decrement the Maslov index by 1 for each tunneling segment along an orbit. If a tunneling segment follows another tunneling segments rather than a classical segment, this decrement of the Maslov index may be attributed to a turning point crossed from within the forbidden region. Thus, the Maslov index of the orbit $\{n;a_0,b_1,\ldots,a_n,b_{n+1}\}$ is given by

$$\mu\{n;a_0,b_1,\ldots,a_n,b_{n+1}\}=2\sum_{k=0}^{n}a_k-\sum_{k=1}^{n+1}b_k\ . \tag{2.6}$$

The parametrized orbits of Eq. (2.4) include not only periodic orbits from A to A, but also "unperiodic" orbits from A to B. Clearly, the orbit $\{n;a_0,b_1,\ldots,a_n,b_{n+1}\}$ is a periodic orbit if and only if the total number of its tunneling segments, $\sum_k b_k$, is even. To insure that only periodic orbits contribute to the complex periodic orbit sum, we multiply the contribution of each orbit by the expression

$$\tfrac{1}{2}\sum_{m=0}^{1}\exp\left[-im\pi\sum_k b_k\right]\ . \tag{2.7}$$

Equation (2.7) is equal to 1 if $\sum_k b_k$ is even, and vanishes if $\sum_k b_k$ is odd.

Substituting Eq. (2.5) for the actions and Eq. (2.6) for the Maslov indices into Eq. (2.3), summing over the parametrized orbits of Eq. (2.4), and introducing the coefficients of Eq. (2.7), we obtain the complex periodic orbit sum for the symmetric double well,

$$g_{\rm sc}(E)=\frac{2T}{i}\sum_{n=0}^{\infty}\sum_{a_0=0}^{\infty}\sum_{a_1,\ldots,a_n=1}^{\infty}\sum_{b_1,\ldots,b_n=1}^{\infty}\sum_{b_{n+1}=0}^{\infty}\tfrac{1}{2}\sum_{m=0}^{1}\exp\left[-im\pi\sum_k b_k\right]$$
$$\times\exp\left[iS\sum_k a_k-\theta\sum_k b_k-\frac{i\pi}{2}\left[2\sum_k a_k-\sum_k b_k\right]\right]\ . \tag{2.8}$$

The number of primitive periodic orbits, f in Eq. (2.3), is equal to two. We may rearrange the phase factors in Eq. (2.8) to obtain a product of geometric series in the a_k and b_k, as follows:

$$g_{\rm sc}(E)=\frac{2T}{i}\tfrac{1}{2}\sum_{m=0}^{1}\sum_{n=0}^{\infty}\sum_{a_0=0}^{\infty}\sum_{a_1,\ldots,a_n=1}^{\infty}\{\exp[ia_0(S-\pi)]\cdots\exp[ia_n(S-\pi)]\}$$
$$\times\sum_{b_1,\ldots,b_n=1}^{\infty}\sum_{b_{n+1}=0}^{\infty}(\exp\{-b_1[\theta+i(m-\tfrac{1}{2})\pi]\}\cdots$$
$$\times\exp\{-b_{n+1}[\theta+i(m-\tfrac{1}{2})\pi]\})\ .$$

Keeping in mind that a_0 and b_{n+1} range from 0 to ∞, while a_k and b_k, for $1 \le k \le n$, range from 1 to ∞, we sum the series and obtain

$$g_{sc}(E)=\frac{T}{i}\sum_{m=0}^{1}\frac{1}{1+e^{iS}}\frac{1}{1-i(-1)^m e^{-\theta}} \times \sum_{n=0}^{\infty}\left[\frac{-e^{iS}}{1+e^{iS}}\frac{i(-1)^m e^{-\theta}}{1-i(-1)^m e^{-\theta}}\right]^n .$$

The sum over n is now a geometric series as well. Performing the sum, we get

$$g_{sc}(E)=\frac{T}{i}\sum_{m=0}^{1}[1+e^{iS}-i(-1)^m e^{-\theta}]^{-1} . \tag{2.9}$$

According to Eq. (2.9), the poles of $g_{sc}(E)$ are the solutions of the equation

$$e^{iS(E)}=-1+i(-1)^m e^{-\theta(E)} ,$$

where we have indicated the energy dependencies explicitly. If E is real, the left side of this equation has modulus one, while the right side has modulus greater than one. We may conclude that the poles of $g_{sc}(E)$ are necessarily complex. It turns out that if the Maslov phase shifts of $\pi/2$ are replaced by the WKB barrier transmission and reflection coefficients, the complex periodic orbit sum yields not only real energies for the poles of $g_{sc}(E)$, but the uniform WKB expressions for the splittings, valid for energies up to the top of the barrier. Here, we shall take a simpler approach, and obtain approximate real poles of $g_{sc}(E)$ in the limit of small tunneling amplitude.

If the tunneling amplitude $e^{-\theta}$ in Eq. (2.9) is neglected, the poles of $g_{sc}(E)$ are the EBK-quantized energies, E_k, given by the condition

$$S(E_k)=2\pi(k+\tfrac{1}{2}) ,$$

where k is an integer. Let us expand $g_{sc}(E)$ about an EBK energy E_k. Note that dS/dE is the period T, so that

$$S(E)=2\pi(k+\tfrac{1}{2})+T(E-E_k)+O(E-E_k)^2 .$$

We substitute this expression into Eq. (2.9) and regard $e^{-\theta}/T$ as a quantity of order $(E-E_k)$. Then to first order in $(E-E_k)$,

$$g_{sc}(E)=\sum_{m=0}^{1}\left[E-\left[E_k-\frac{(-1)^m e^{-\theta}}{T}\right]\right]^{-1} .$$

Finally, let us sum over the quantum number k to obtain

$$g_{sc}(E)=\sum_k\left\{\left[E-\left[E_k-\frac{e^{-\theta}}{T}\right]\right]_{m=0}^{-1}+\left[E-\left[E_k+\frac{e^{-\theta}}{T}\right]\right]_{m=1}^{-1}\right\} . \tag{2.10}$$

The approximate poles of $g_{sc}(E)$ are the EBK energies E_k, split by the tunneling energies $e^{-\theta}/T$. The poles have unit strength, so the associated energy levels are nondegenerate. From quantum mechanics, we know that the eigenstates associated with the energy doublet $E_k \pm e^{-\theta}/T$ have definite parities. The state with lower energy has even parity, while the state with higher energy has odd parity. In Eq. (2.10) we have explicitly identified the $(m=0)$ and $(m=1)$ terms from the sum over m. Note that the $(m=0)$ term contributes the poles associated with the even parity states, while the $(m=1)$ term contributes the odd parity poles. Note too that the $(m=0)$ and $(m=1)$ poles contain contributions from both the complex periodic orbits from A to A and from the "unperiodic" orbits from A to B. These "unperiodic" orbits contribute in an essential way to the poles of definite parity. We shall discuss this further in Sec. IV C.

Our treatment of the symmetric double well differs in certain respects from Miller's original calculation. We have included a larger family of complex periodic orbits in the sum. The additional orbits render the identification of the poles of $g_{sc}(E)$ more straightforward, and also yield the correct pole strengths. [Miller computed $g_{sc}(E)$ up to a proportionality constant.] The pole strengths are more significant in determining the SF_6 rotational spectrum, which contains degenerate energy levels.

III. ROTATIONAL DYNAMICS OF SF_6

In recent years, a wealth of research has been devoted to the rotational spectra of symmetric molecules. Advances in ultrahigh resolution spectroscopy have revealed fine, superfine, and hyperfine structures of great complexity.[14–18] Theoretical analyses have evolved concomitantly.[19–21] Harter and Patterson, whose treatment combines semiclassical ideas with results from the theory of induced representations, have been particularly successful.[22–25] Several reviews of the field have been written.[28–30]

In this section we describe a model for the rotational dynamics of symmetric molecules. In Sec. III A we present the classical version of the model. The classical discussion has two goals. The first is to provide physical intuition. The second is to lay the ground work for the complex periodic orbit sum, which is based on the classical description of the dynamics. In Sec. III B we discuss the quantum-mechanical version of the model. The purpose of this section is to describe the rich structure of symmetric-molecular rotational spectra, which will be obtained from the complex periodic orbit sum in Sec. IV. As many of the cited studies have done, we will take the octahedrally symmetric molecule SF_6 as our primary example.

A. Classical model

For the consideration of rotational dynamics, we regard the SF_6 molecule as a semi-rigid body. The Hamiltonian

$$H(\mathbf{J})=\alpha J^2+\beta(J_x^4+J_y^4+J_z^4-\tfrac{3}{5}J^4) , \tag{3.1}$$

derived by Hecht,[19] has been used extensively to model the rotational dynamics of molecules with octahedral symmetry. J_x, J_y, and J_z are the components of the

body-fixed angular momentum **J**. The first term in Eq. (3.1) is the usual rigid body Hamiltonian for a spherical top. (The moments of inertia of a rigid body with octahedral symmetry are necessarily equal.) The quartic terms introduce corrections to the rotational energy due to the centrifugal distortion of the molecule. Note that $J_x^4+J_y^4+J_z^4$ and J^4 are the lowest-order polynomials consistent with both octahedral and time-reversal symmetry. These polynomials, with the components of angular momentum replaced by the coordinates x, y, and z, are well known from crystal field theory.[13] The parameters α and β have been fitted to spectroscopic data for SF_6 and are given by $\alpha=0.091\,083\ \text{cm}^{-1}$ and $\beta=54.4$ Hz, or $1.81\times10^{-9}\ \text{cm}^{-1}$.[17,31,32]

The equation of motion for the body-fixed angular momentum is Euler's equation,

$$\dot{\mathbf{J}}=\boldsymbol{\omega}\times\mathbf{J},\quad \boldsymbol{\omega}=-\nabla H\ . \tag{3.2}$$

Euler's equation conserves the total angular momentum J^2. Thus, trajectories are confined to spheres of constant total angular momentum in **J** space. For the remainder of this discussion, we restrict attention to a particular sphere, $|\mathbf{J}|=J$, for some constant J. (The quantum-mechanical analogue of this restriction is to fix the total angular momentum quantum number j.)

Let us consider the qualitative features of the dynamics, in which the octahedral symmetry of the Hamiltonian plays an important role. Consider first the fixed points, which correspond to the uniform rotation of the rigid body about a fixed axis. The Hamiltonian, Eq. (3.1), has six stable fixed points of maximum energy $E_M=\beta J^4$, 12 unstable saddle points with energy $E_s=\beta/2J^4$, and eight stable energy minima with energy $E_m=\beta/3J^4$.

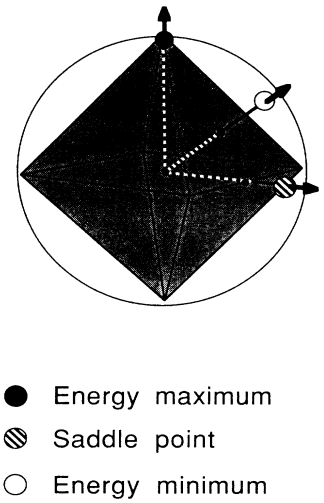

FIG. 2. Fixed points of SF_6 Hamiltonian. An octahedron is inscribed in the sphere of constant angular momentum. Energy maxima lie along axes through the vertices of the octahedron, saddle points along axes through the faces, and energy minima along axes through the edges of the octahedron. Only one of each type of fixed point is shown.

(The energies E_M, E_s, and E_m are quoted relative to the constant energy $\alpha J^2-3/5\beta J^4$.) The positions of the fixed points are indicated in Fig. 2, in which an octahedron is inscribed in the sphere $|\mathbf{J}|=J$. The energy maxima are at the vertices of the octahedron, the saddle points lie along axes bisecting the edges, and the energy minima lie along axes through the faces of the octahedron.

It is easy to understand on physical grounds why the rotational energy maxima and minima are situated as they are for the SF_6 molecule. For fixed total angular momentum, the energy of a rigid body rotating uniformly about a fixed axis is inversely proportional to its moment of inertia about the axis. Imagine the fluorine atoms arranged at the vertices of an octahedron, where they are strongly bound to the sulfur atom at the center, and weakly bound to each other. (It would be more accurate to consider the stretching and bending vibrational modes, but a simple-minded picture will do here.) When the SF_6 molecule rotates about an axis through a vertex of the octahedron, the S—F bonds in the plane of rotation stretch relatively little in response to the centrifugal forces. The increase in the moment of inertia above its equilibrium value is relatively small, and the rotational energy decreases relatively little. When the molecule rotates about an axis through a face of the octahedron, the weaker F—F bonds in the plane of rotation are stretched more by the centrifugal forces. The increase in moment of inertia is relatively large, and the rotational energy decreases relatively more.

We consider next the periodic orbits of the system. The periodic orbits are contours of constant energy on the sphere $|\mathbf{J}|=J$. Both the number and the disposition of these orbits depend on the energy. At energies greater than the saddle-point energy E_s, there are six periodic orbits, which encircle the six energy maxima. These orbits are shown in Fig. 3(a); they correspond to the precession of the body-fixed angular momentum about an axis of maximum energy. The orbits are mapped into each other by octahedral rotations. As a special case, each orbit is invariant under a rotation by $\pi/2$ about its center. Following Harter and Patterson, we refer to these as *fourfold orbits*. At energies less than the saddle-point energy E_s, there are eight periodic orbits encircling the eight energy minima, which are shown in Fig. 3(b). These orbits correspond to the precession of the body-fixed angular momentum about an axis of minimum energy. They are also mapped into one another by octahedral rotations. In particular, each orbit is invariant under a rotation by $2\pi/3$ about its center. We will refer to these as *threefold orbits*. The orbits with energy equal to E_s are the separatrices. For this reason, we will often refer to E_s as the separatrix energy. The separatrices join the saddle points. The threefold, fourfold, and separatrix orbits are illustrated in Fig. 3(c). [Figures 2 and 3 may be regarded as simplified versions of the rotational energy (RE) surface, a graphical representation of rotational dynamics developed by Harter.[25,30]]

The complex periodic orbit sum, Eq. (2.3) is based on a canonical description of the classical dynamics. In particular, it requires the canonical actions of the periodic orbits, real and complex. Therefore, the equation of

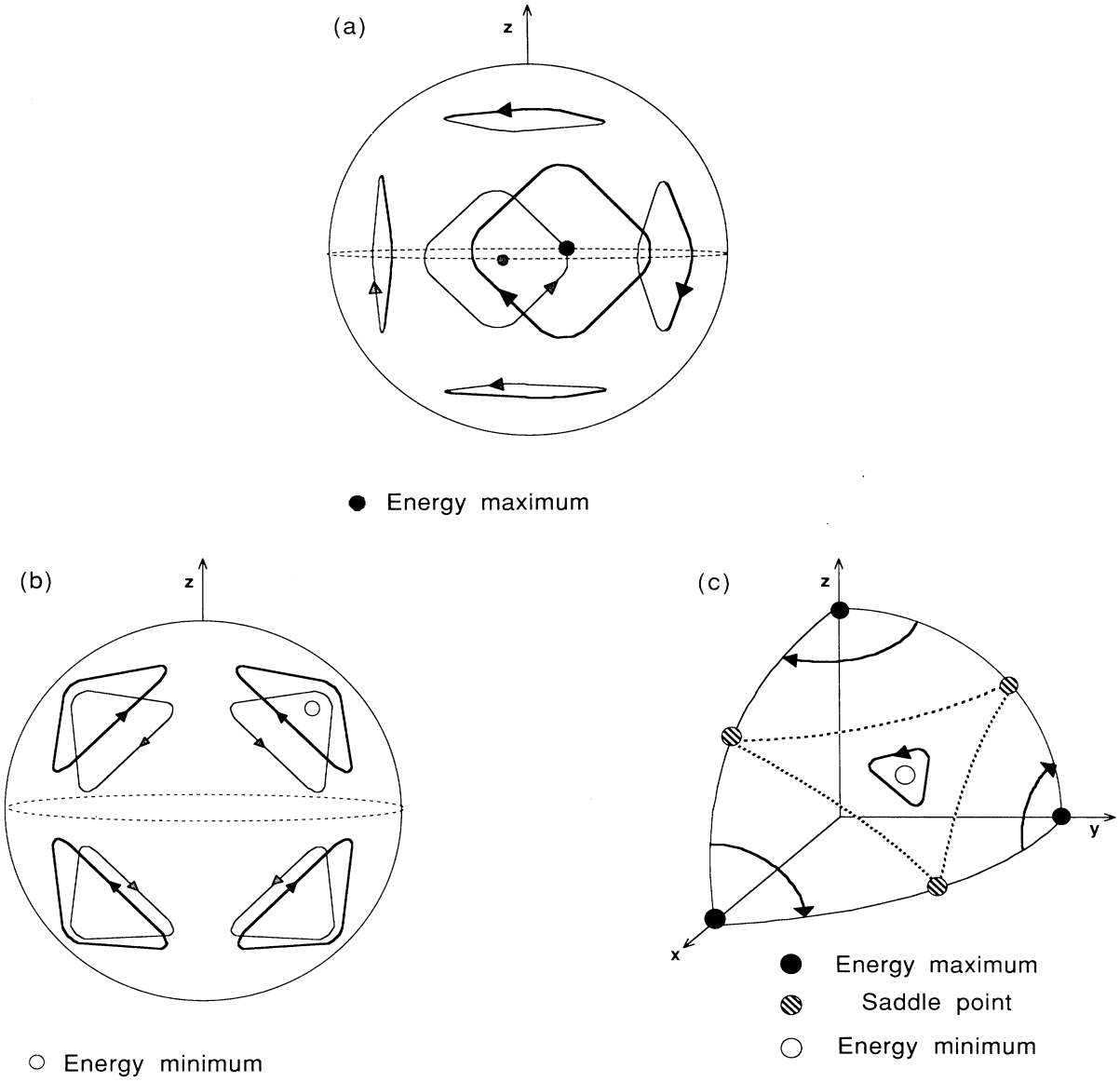

FIG. 3. Periodic orbits of SF_6 Hamiltonian. (a) $E > E_s$. Six orbits encircle the energy maxima clockwise. Only one energy maximum is shown. (b) $E < E_s$. Eight orbits encircle the energy minima counterclockwise. Only one energy minimum is shown. (c) Portions of orbits of different energies on an octant of the constant angular momentum sphere. The separatrix orbit joins the saddle points.

motion, Eq. (3.2), must be cast in canonical form. The variables ϕ and $J_z = J\cos\theta$, where (θ,ϕ) are spherical coordinates on the sphere $|\mathbf{J}| = J$, serve as canonical coordinates. That is,

$$\{\phi, J_z\} = -1 \ . \tag{3.3}$$

Equation (3.3) may be regarded as the definition of the Poisson bracket on the sphere $|\mathbf{J}| = J$, which we now regard as a classical phase space. If the Hamiltonian H and the body-fixed angular momentum $\mathbf{J}$ are expressed in terms of J_z and ϕ, the canonical equation of motion $\dot{\mathbf{J}} = \{\mathbf{J}, H\}$ is equivalent to Euler's equation. Motivated by Eq. (3.3), we take the action differential dS to be

$$dS = -J_z d\phi = -J\cos\theta \, d\phi \ . \tag{3.4}$$

The minus sign in Eqs. (3.3) and (3.4) has its origin in the commutation relations of the body-fixed angular momentum.

B. Quantum model: The rotational spectrum of SF_6

To obtain a quantum-mechanical description of the rotational dynamics of SF_6, we must transform the classical Hamiltonian into a quantum-mechanical operator. This "quantization procedure" is beset with the usual ordering ambiguities. We have studied a well-defined mapping between classical and quantum-mechanical observables for

rotational systems, analogous to the Wigner-Weyl correspondence and hope to discuss it in a future publication. For present purposes, we simply replace classical variables with quantum-mechanical operators. Thus, the quantum-mechanical Hamiltonian $\hat{H}$ is given by

$$\hat{H}=\alpha\hat{J}^2+\beta[\hat{J}_x^4+\hat{J}_y^4+\hat{J}_z^4-\tfrac{1}{5}(\hat{J}^2)^2] , \tag{3.5}$$

where $\hat{J}_x$, $\hat{J}_y$, and $\hat{J}_z$ are the body-fixed angular momentum operators.

Because the body-fixed angular momentum operators do not mix states with different total angular momentum, $\hat{H}$ can be restricted without approximation to a finite-dimensional subspace of fixed total angular momentum. To demonstrate this more explicitly, it is convenient to introduce the $|jmk\rangle$ basis states for the rigid body Hilbert space. The $|jmk\rangle$ states are simultaneous eigenstates of the total angular momentum $\hat{J}^2$, the z component of space-fixed angular momentum $\hat{j}_z$, and the z component of body-fixed angular momentum $\hat{J}_z$. The eigenvalues of these three operators acting on the state $|jmk\rangle$ are $j(j+1)$, m, and k, respectively, where $j=0,1,\ldots$ and $-j\le m,k\le j$. Since $\hat{J}^2$ and $\hat{j}_z$ commute with $\hat{H}$, we can restrict $\hat{H}$ to the $(2j+1)$-dimensional subspace spanned by the states $|jmk\rangle$ with fixed j and m. On this subspace, $\hat{H}$ is represented by the matrix $H_{kk'}=\langle jmk|\hat{H}|jmk'\rangle$, and its spectrum can be obtained by diagonalizing this matrix. Fox *et al.* computed the spectrum of $\hat{H}$ for $j=1,\ldots,100$,[21] and pointed out many features of the fine and superfine structure of $\hat{H}$ that we will presently describe. For the remainder of this discussion, we regard j and m as fixed, and regard $\hat{H}$ as a $(2j+1)\times(2j+1)$ matrix. We confine ourselves to the case of integral j.

Let us address first the symmetries and spectral degeneracies which can be anticipated on the basis of standard group theory. $\hat{H}$ has octahedral symmetry. Its $(2j+1)$ eigenvectors belong to degenerate subspaces which carry irreducible representations, or irreps, of the octahedral group. The octahedral group has five irreps. It has two one-dimensional irreps A_1 and A_2, a two-dimensional irrep E, and two three-dimensional irreps T_1 and T_2. In the absence of accidental degeneracies, the eigenvalues of $\hat{H}$ are either nondegenerate, doubly degenerate, or triply degenerate. Each eigenvalue may be labeled by the irrep carried by its eigenspace.

There is considerable structure in the SF_6 rotational spectrum beyond the degeneracies produced by octahedral symmetry. With increasing j, the eigenvalues coalesce to form nearly degenerate clusters. Clusters with energies greater than the classical separatrix energy E_s contain precisely six levels, degeneracies counted, while clusters with energies less than E_s contain precisely eight levels, degeneracies counted. The *fine structure* refers to the splitting between adjacent clusters. At j values for which the model Hamiltonian $\hat{H}$ is valid, the fine-structure splitting is much smaller than the separations between energy levels with different j. Using the values of α and β quoted above, the difference in the spherical top energies, $\alpha j(j+1)$, of the $j=30$ and $j=31$ multiplets is about 5 cm^{-1}, while the fine-structure splittings within the $j=30$ multiplet are on the order of 10^{-4} cm^{-1}.

We will use the terminology of Hartree and Patterson, and refer to clusters of six levels as *fourfold clusters*, and clusters of eight levels as *threefold clusters*. The terminology has its origins in their semiclassical analysis, as there is a correspondence between the fourfold clusters in the quantum spectrum and the fourfold classical orbits discussed in Sec. III A, and an analogous correspondence between the threefold clusters and the threefold orbits.[25]

One of the most remarkable features of the clusters is the regularity and periodicity of their irrep content. Among the fourfold clusters, one finds a cluster containing an A_1, T_1, and E level. (Note that the number of levels in the cluster, degeneracies counted, is $1+3+2=6$.) With decreasing energy, it is followed by a cluster containing a T_2 and T_1 level, which is followed by a cluster containing an E, T_2, and A_2 level, which is followed by a cluster containing a T_2 and T_1 level. This cycle of clusters then repeats itself down to energies close to E_s. There the pattern is interrupted, as the fourfold clusters merge with the threefold clusters. Figure 4(a) illustrates the cycle of fourfold clusters. The clusters are assigned indices 0, 1, 2, and 3, which correspond to the order in which they appear. The cycle begins with the fourfold cluster of highest energy; its index is given by

$$j \bmod 4 . \tag{3.6}$$

For example, if $j=30$, then $j \bmod 4=2$, and the cluster with highest energy contains an E, T_2, and A_2 level.

A similar pattern exists for the threefold clusters. One finds among them a cluster containing an A_2, T_2, T_1, and A_1 level. (Note that the number of levels in the cluster, degeneracies counted, is $1+3+3+1=8$.) With increasing energy, it is followed by two clusters containing a T_1, E, and T_2 level. This cycle of clusters then repeats itself up to energies close to E_s. There the pattern is interrupted, as the threefold clusters merge with the fourfold clusters. Figure 4(b) illustrates the cycle of threefold clusters; the three clusters in the sequence are labeled by indices 0, 1, and 2. The cycle begins with the cluster of lowest energy; its index is given by

$$j \bmod 3 . \tag{3.7}$$

Thus, if $j=30$, the $j \bmod 3=0$, and the cluster with lowest energy contains an A_1, T_1, T_2, and A_2 level.

The *superfine structure* refers to the splitting between the levels within a cluster. For most clusters, the superfine splitting is much smaller than the fine splitting. Indeed, it is this separation of scales that enables one to identify the clusters in the first place. For a few energy levels in the middle of the spectrum, the two splittings are of the same order of magnitude. These levels span a transition between the fourfold clusters and the threefold clusters. In effect, two clusters of each type overlap, and the levels in question are shared by both.

The superfine structure introduces additional structure in the irrep content of the clusters. It turns out that the levels in the clusters occur in a definite sequence which depends on the parity of j. As an example, consider the

fourfold cluster of index 0, for the case of even j. The A_1 level has the highest energy, followed by the T_1 level, followed by the E level. The other sequences are described in Figs. 4(a) and 4(b). For odd j, the ordering of the levels within the clusters is reversed. Let us point out a final remarkable feature of the superfine structure. The superfine splittings approximately obey certain simple ratios. As an example, consider the fourfold cluster of index 0, for the case of j even. The splittings of the three levels A_1, T_1, and E from their degeneracy-weighted mean are in the ratio 2:0:−1. When j is odd, the signs of the splitting ratios are reversed. The splitting ratios for the other clusters are given in Figs. 4(a) and 4(b).

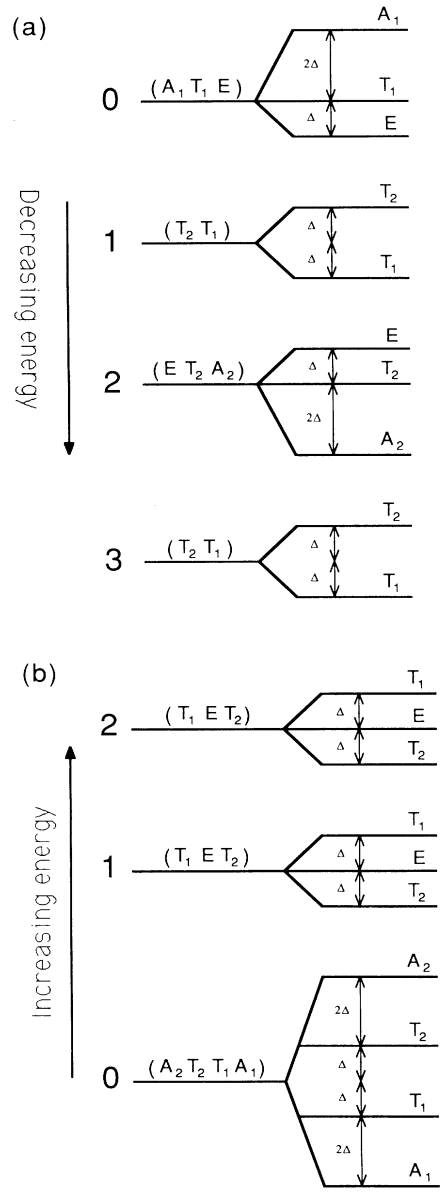

FIG. 4. Clusters and superfine splitting. The irrep content, ordering, and the relative splitting Δ of the superfine clusters is shown. (a) Fourfold clusters, indexed by 0, 1, 2, and 3. (b) Threefold clusters, indexed by 0, 1, and 2.

Harter and Patterson have developed a semiclassical theory which explains the qualitative features of the SF_6 rotational spectrum, and which is in good quantitative agreement with quantum-mechanical calculations. The fine-structure levels are obtained from the Bohr-Sommerfeld quantization rule. The patterns and periodicity in the irrep labels are explained on the basis of the Frobenius reciprocity theorem. Their treatment is not fully semiclassical, however, in that the superfine splittings are obtained by diagonalizing a nearly degenerate block of the quantum Hamiltonian. (The matrix elements are determined from semiclassical information.) In Sec. IV we obtain similar results using a very different method, namely, sums over complex classical periodic orbits. The treatment is fully semiclassical, and involves no quantum-mechanical computations, such as matrix diagonalizations.

IV. CALCULATION

In this section we apply the complex periodic orbit sum, Eq. (2.3) to the SF_6 model Hamiltonian discussed in Sec. III. Throughout, we set $\hbar=1$. In Sec. IV A, we consider energies greater than the classical separatrix energy E_s, and in Sec. IV B, energies less than E_s. The two cases must be treated separately because the topology of the complex energy shell is different in each case. The calculation for $E>E_s$ is carried out in detail, and it parallels the double well calculation of Sec. II B. The main result is Eqs. (4.9) and (4.10), which give the fine and superfine structure for the fourfold clusters. The presentation of Sec. IV B is considerably condensed. The main result is Eq. (4.14), which gives the fine and superfine structure for the threefold clusters. In Sec. IV C we discuss a surprising result of the periodic orbit calculations, namely, the determination of the symmetry labels of the energy eigenvalues.

A. Case $E>E_s$

The complex energy shell is the stage on which the complex periodic orbit sum is performed. For this problem, it is a two-dimensional surface in complex **J** space given by the intersection of the surfaces $\mathbf{J}\cdot\mathbf{J}=J^2$ and $H(\mathbf{J})=E$. [H is the rotational Hamiltonian of Eq. (3.1).] As it turns out, we will have no need to work with the complex energy shell directly. For energies $E>E_s$, we claim that it is topologically equivalent to the "chicken wire mesh," or spherical lattice shown in Fig. 5(a). The six rings of the lattice are the fourfold periodic orbits discussed in Sec. III A and shown in Fig. 3(a). These orbits are the primitive periodic orbits of the complex energy shell. In Fig. 5(a) 24 nodes stud the orbits, four to an orbit. The nodes are obtained by applying the octahedral rotations to the node A. We will take A to be the base point of the complex perodic orbits in the sum. We take the classical segments to be one-quarter cycles of the fourfold orbits, with nodes as endpoints. An example is the path from A to C, shown in Fig. 5(a). Joining each fourfold orbit to its four nearest neighbors are tunneling

segments. An example is the path from A to B in Fig. 5(a). There are, in fact, two topologically distinct tunneling segments between each pair of neighboring orbits, along which the action differential dS is either positive or negative imaginary, although only one is shown in Fig. 5(a).

In accordance with the prescription of Sec. II A, we sum over paths on the lattice which begin at A, pass from node to node along classical and tunneling segments, and then return to A. (These paths are the special representative orbits.) Classical segments must be traversed in the sense determined by Euler's equation, that is, clockwise. Tunneling between neighboring orbits must occur along the tunneling segment for which the action $\int dS$ is positive imaginary. With these restrictions, it is clear that at each node a path can continue in one of two ways. It can orbit clockwise, or else it can tunnel along one of the two tunneling segments. Therefore, we may adopt the parametrization of Eq. (2.4), and describe the paths by an alternating sequence of classical and tunneling episodes. As in Sec. II B, the sequence $\{n;a_0,b_1,\ldots,a_n,b_{n+1}\}$ corresponds to a path which consists of a_0 classical segments, followed by b_1 tunneling segments , . . . , followed by a_n classical segments, followed by b_{n+1} tunneling segments. Of course, most of the parametrized paths $\{n;a_0,b_1,\ldots,a_n,b_{n+1}\}$ are not periodic, and terminate at some node other than A. For the moment, we defer the problem of identifying the periodic orbits from among the parametrized paths, and determine their actions and Maslov indices first.

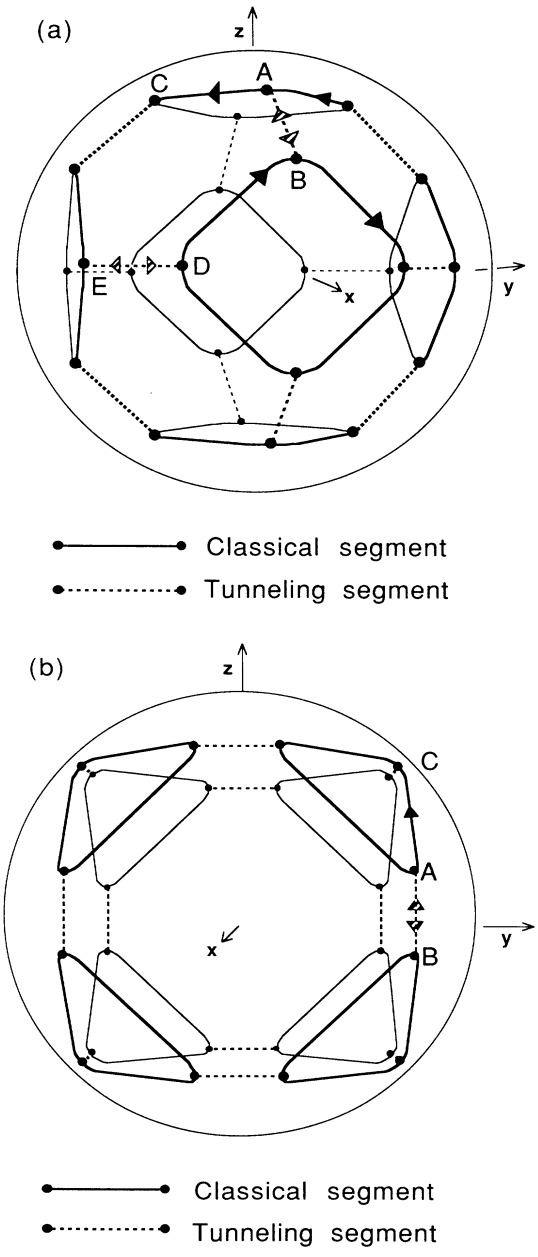

FIG. 5. Complex energy shell for SF_6 Hamiltonian. (a) $E > E_s$. Tunneling segments join the real periodic orbits to their four nearest neighbors. (b) $E < E_s$. Tunneling segments join the real periodic orbits to their three nearest neighbors.

The action differential dS of Eq. (3.4) is proportional to the magnitude of the classical angular momentum J. To obtain agreement with quantum-mechanical results we must quantize J. We impose the quantization condition

$$J=(j+\tfrac{1}{2}) , \tag{4.1}$$

where j is the total angular momentum quantum number. An alternative quantization condition, used by Harter and Patterson,[25] is to take $J=\sqrt{j(j+1)}$. Note that this condition differs from Eq. (4.1) by terms of relative order $1/j^2$. Substituting Eq. (4.1) into Eq. (3.4), we obtain

$$dS=-(j+\tfrac{1}{2})\cos\theta d\phi . \tag{4.2}$$

The action Γ and Maslov index μ of the parametrized paths are obtained by adding up the actions and Maslov index adjustments along individual segments. Both the formulas for Γ and μ, Eqs. (A1) and (A2), and their derivations are more complicated than the analogous ones, Eqs. (2.5) and (2.6), for the double well. They are obtained in the Appendix. For the complex periodic orbit sum, we require only the total phase $\Gamma-\mu\pi/2$ of the parametrized paths, which is given by the following equation, Eq. (A3) in the Appendix:

$$\left[\Gamma-\frac{\pi}{2}\mu\right]\{n;a_0,b_1,\ldots,a_n,b_{n+1}\} = \frac{S}{4}\sum_{k=0}^{n}a_k+[i\theta-(j+\tfrac{1}{2})\pi]\sum_{k=1}^{n+1}b_k .$$

Here, S is the action taken around the fourfold orbit encircling the north pole, and $i\theta$ is the action taken along a tunneling path chosen so that θ is positive. We see that each classical segment contributes $S/4$ to the total phase, and each tunneling segment contributes $i\theta-(j+1/2)\pi$. The term $(j+1/2)\pi$ is due to the Maslov index.

It remains to identify the periodic orbits from among the parametrized paths. We determine first the node at which the path $\{n;a_0,b_1,\ldots,a_n,b_{n+1}\}$ terminates. Observe that the classical and tunneling segments can be

generated by octahedral rotations. As an example, consider the base point A in Fig. 5(a). The classical segment at A goes to the node C, which is obtained from A by a rotation about the z axis by $-\pi/2$. Let ω denote this operation,

$$\omega = R_z(-\pi/2) \ . \tag{4.3a}$$

The tunneling segment at A goes to the node B, which is obtained from A by a rotation about the z axis by π, followed by a rotation about the y axis by $\pi/2$. Let τ denote this operation,

$$\tau = R_y(\pi/2)R_z(\pi) \ . \tag{4.3b}$$

At nodes other than A, there are different rotations which generate the classical and tunneling segments. However, these are related to ω and τ by conjugation. For example, at the node $g\cdot A$, obtained by applying the octahedral rotation g to A, the classical and tunneling segments are generated by $g\omega g^{-1}$ and $g\tau g^{-1}$, respectively. Thus, the parametrized paths can be generated by applying a sequence of rotations of the forms $g\omega g^{-1}$ and $g\tau g^{-1}$ to the base point A. It is straightforward to show that the path $\{n;a_0,b_1,\ldots,a_n,b_{n+1}\}$ terminates at the node obtained by applying the rotation $\omega^{a_0}\tau^{b_1}\cdots\omega^{a_n}\tau^{b_{n+1}}$ to A. Therefore, the path $\{n;a_0,b_1,\ldots,a_n,b_{n+1}\}$ is periodic if and only if

$$\omega^{a_0}\tau^{b_1}\cdots\omega^{a_n}\tau^{b_{n+1}} = I \ ,$$

where I is the identity element of the octahedral group.

It is a standard result from group theory that the δ function at the identity can be expressed as a sum over the characters of the irreducible representations.[33] Let $\chi_m(g)$ denote the character of the mth irreducible representation of the octahedral group, and let d_m be its dimensionality. Then the expression

$$\delta(g;I) = \tfrac{1}{24}\sum_m d_m\chi_m(g)$$

is equal to 1 if g is the identity, and vanishes otherwise. To insure that only periodic orbits contribute to the complex periodic orbit sum, we multiply the contribution of each parametrized path by the expression

$$\tfrac{1}{24}\sum_m d_m\chi_m(\omega^{a_0}\tau^{b_1}\cdots\omega^{a_n}\tau^{b_{n+1}}) \ . \tag{4.4}$$

Let us note that the δ function, Eq. (4.4), is completely analogous to Eq. (2.7) of the double well calculation,

$$\tfrac{1}{2}\sum_{m=0}^{1}\exp\left[-im\pi\sum_k b_k\right] \ .$$

Indeed, Eq. (2.7) may be interpreted as a sum over the characters of the cyclic group C_2. C_2 contains two elements: the identity I, which generates the classical segments in the double well, and the reflection R, which generates the tunneling segments. C_2 has two irreducible representations: the trivial representation, labeled by $m=0$, and the repreesntation which assigns 1 to I and -1 to R, labeled by $m=1$. The phase factor $\exp(-im\pi\sum_k b_k)$ is just the character χ_m evaluated at the group element $I^{a_0}R^{b_1}\cdots I^{a_n}R^{b_{n+1}}$, and the sum in Eq. (2.7) is just the group δ function, $\delta(I^{a_0}R^{b_1}\cdots I^{a_n}R^{b_{n+1}};\mathcal{I})$.

Substituting Eq. (A3) for the actions and Maslov indices into Eq. (2.3), summing over the parametrized paths of Eq. (2.4), and introducing the coefficients of Eq. (4.4), we obtain the complex periodic orbit sum for the SF_6 Hamiltonian,

$$g_{\rm sc}(E) = \frac{6T}{i}\sum_{n=0}^{\infty}\sum_{a_0=0}^{\infty}\sum_{a_1,\ldots,a_n=1}^{\infty}\sum_{b_1,\ldots,b_n=1}^{\infty}\sum_{b_{n+1}=0}^{\infty}\tfrac{1}{24}\sum_m d_m\chi_m(\omega^{a_0}\tau^{b_1}\cdots\omega^{a_n}\tau^{b_{n+1}})$$

$$\times\exp\left[(iS/4)\sum_k a_k - [\theta + i(j+\tfrac{1}{2})\pi]\sum_k b_k\right] \ . \tag{4.5}$$

The number of primitive periodic orbits, f in Eq. (2.3), is equal to six, and T is the period of these orbits. To proceed, we express the character $\chi_m(g)$ as the trace of the irreducible matrix representative, $\underline{D}_m(g)$. Using the representation property $\underline{D}_m(gg') = \underline{D}_m(g)\underline{D}_m(g')$, we have that

$$\chi_m(\omega^{a_0}\tau^{b_1}\cdots\omega^{a_n}\tau^{b_{n+1}}) = \mathrm{Tr}[\underline{D}_m(\omega)^{a_0}\underline{D}_m(\tau)^{b_1}\cdots\underline{D}_m(\omega)^{a_n}\underline{D}_m(\tau)^{b_{n+1}}] \ . \tag{4.6}$$

We substitute Eq. (4.6) into Eq. (4.5), and rearrange phase factors so as to obtain a product of geometric series in the a_k and b_k. Then

$$g_{\rm sc}(E) = \frac{6T}{i}\frac{1}{24}\sum_m d_m\sum_{n=0}^{\infty}\sum_{a_0=0}^{\infty}\sum_{a_1,\ldots,a_n=1}^{\infty}\sum_{b_1,\ldots,b_n=1}^{\infty}\sum_{b_{n+1}=0}^{\infty}\mathrm{Tr}\{[e^{iS/4}\underline{D}_m(\omega)]^{a_0}[e^{-\theta-i(j+1/2)\pi}\underline{D}_m(\tau)]^{b_1}\cdots$$

$$\times[e^{iS/4}\underline{D}_m(\omega)]^{a_n}[e^{-\theta-i(j+1/2)\pi}\underline{D}_m(\tau)]^{b_{n+1}}\} \ .$$

The terms in the series are matrices. We sum the series, keeping in mind that a_0 and b_{n+1} range from 0 to ∞, while a_k and b_k, for $1 \le k \le n$, range from 1 to ∞. As in the double well calculation, the sum over n becomes a geometric series which is easily carried out. We obtain finally

$$g_{sc}(E)=\frac{T}{4i}\sum_m d_m \mathrm{Tr}\{[\underline{I}_m - e^{iS/4}\underline{D}_m(\omega) + i(-1)^j e^{-\theta}\underline{D}_m(\tau)]^{-1}\} . \quad (4.7)$$

Equation (4.7) is a closed-form, semiclassically approximate expression for the trace of the energy-dependent Green's function $g_{sc}(E)$. It depends on the classical action S of the primitive periodic orbits, their Maslov indices, which manifest themselves in the phase factor $i(-1)^j$, the tunneling action θ, and the irreducible matrix representatives of the generators of the classical and tunneling segments, $\underline{D}_m(\omega)$ and $\underline{D}_m(\tau)$. As we shall see, Eq. (4.7) contains all of the structure of the SF_6 rotational spectrum described in Sec. III B. Similar expressions can be obtained for other rotational Hamiltonians.

To obtain the poles of $g_{sc}(E)$ explicitly, we need to substitute actual matrices for $\underline{D}_m(\omega)$ and $\underline{D}_m(\tau)$, where ω and τ are given by Eq. (4.3). While the irreducible matrix representatives of the octahedral group are not often found in the standard references, it is a straightforward matter to construct them.[34] Substituting these matrices into Eq. (4.9), we obtain an explicit expression for $g_{sc}(E)$. One finds that this expression has complex poles, as does Eq. (2.9) for the double well. We make the same approximation we used earlier. In the limit of vanishing tunneling amplitude, the poles of $g_{sc}(E)$ are the EBK-quantized energies E_k, determined by the condition

$$S(E_k)=2\pi k . \quad (4.8)$$

We expand $g_{sc}(E)$ about the EBK energies, taking denominators to first order in the tunneling amplitude and numerators to zeroth order. Summing over the EBK quantum number k, we obtain

$$g_{sc}(E)=\sum_k \left[\left[\frac{1}{(1-i^k)C+i^k(E-E_k)-4(-1)^j e^{-\theta}}\right]_{A_1} + \left[\frac{1}{(1+i^k)C-i^k(E-E_k)+4(-1)^j e^{-\theta}}\right]_{A_2} + \left[\frac{2}{(1-\sigma_k)C/2+\sigma_k(E-E_k)+2i^k(-1)^j e^{-\theta}}\right]_{E} + \left[\frac{3(3-2i^k+\sigma_k)}{(1-i^k)(1+\sigma_k)C+[i^k-2\sigma_k+3(-i)^k](E-E_k)+4(1-i^k)(-1)^j e^{-\theta}}\right]_{T_1} + \left[\frac{3(3+2i^k+\sigma_k)}{(1+i^k)(1+\sigma_k)C-[i^k+2\sigma_k+3(-i)^k](E-E_k)-4(1+i^k)(-1)^j e^{-\theta}}\right]_{T_2}\right] ,$$

where

$$\sigma_k=(-1)^k \text{ and } C=\frac{4i}{T} . \quad (4.9)$$

Equation (4.9) is our final result for the trace of the energy-dependent Green's function $g_{sc}(E)$ for the SF_6 Hamiltonian at energies above the classical separatrix energy E_s. The expression is complicated, but then the spectrum it is intended to describe is complicated as well. Note that we have labeled the terms in the expression by irreps of the octahedral group. In effect, we have explicitly identified the terms from the sum over irreps in Eq. (4.7). We will assign these irrep labels to the energy levels obtained from Eq. (4.9). That is, poles in the first term of Eq. (4.9) will be labeled by A_1, poles in the second term by A_2, etc. Although the complex periodic orbit prescription does not indicate that these irrep assignments are warranted, they turn out to be correct.

Let us determine the poles in the neighborhood of an EBK energy E_k. Examination of Eq. (4.9) reveals that the pole structure depends on the value of (k mod4); the singular terms are those in which the coefficient of C vanishes for a given k. Consider first the case where (k mod4=0). Then $g_{sc}(E)$ is given by

$$g_{sc}(E)=\left[\frac{1}{E-[E_k+4(-1)^j e^{-\theta}/T]}\right]_{A_1} + \left[\frac{3}{E-E_k}\right]_{T_1} + \left[\frac{2}{E-[E_k-2(-1)^j e^{-\theta}/T]}\right]_{E} + \cdots , \quad k \bmod 4=0 , \quad (4.10a)$$

where the ellipsis represents finite terms that consist of nonsingular contributions to $g_{sc}(E)$. Equation (4.10a) predicts a nondegenerate level with energy $E_k+4(-1)^j e^{-\theta}/T$ and irrep label A_1, a triply degenerate level with energy E_k and irrep label T_1, and a doubly degenerate level with energy $E_k-2(-1)^j e^{-\theta}/T$ and irrep label E. Note that the degeneracies, which are determined by the pole strengths, are consistent with the irrep labels. Let us compare these results with the spectra of Fig. 4(a). Evidently, Eq. (4.10a) describes the structure of the fourfold cluster of index 0. The irrep labels appear in the correct order. The splitting ratios are reproduced. The sign of the splitting exhibits the correct dependence on the parity of j. Furthermore, we see that the mean energy of the cluster is E_k, and the splitting Δ is given by $2(-1)^j e^{-\theta}/T$.

Consider next the case (k mod4=1). Then $g_{sc}(E)$ is

given by

$$g_{sc}(E)=\left[\frac{3}{E-[E_k+2(-1)^j e^{-\theta}/T]}\right]_{T_2}+\left[\frac{3}{E-[E_k-2(-1)^j e^{-\theta}/T]}\right]_{T_1}+\cdots,$$
$$k \bmod 4=1 . \quad (4.10b)$$

According to Eq. (4.10b), there is a triply degenerate level with energy $E_k+2(-1)^j e^{-\theta}/T$ and irrep label T_2, and a triply degenerate level with energy $E_k-2(-1)^j e^{-\theta}/T$ and irrep label T_1. Evidently, Eq. (4.10b) describes the fourfold clusters of index 1, in which the mean energy of the cluster is E_k, and the splitting Δ is given by $2(-1)^j e^{-\theta}/T$. Finally, consider the remaining cases (k mod4=2) and (k mod4=3). Then $g_{sc}(E)$ is given by

$$g_{sc}(E)=\left[\frac{2}{E-[E_k+2(-1)^j e^{-\theta}/T]}\right]_{E}+\left[\frac{3}{E-E_k}\right]_{T_2}+\left[\frac{1}{E-[E_k-4(-1)^j e^{-\theta}/T]}\right]_{A_2}+\cdots,$$
$$k \bmod 4=2 , \quad (4.10c)$$

and

$$g_{sc}(E)=\left[\frac{3}{E-[E_k+2(-1)^j e^{-\theta}/T]}\right]_{T_2}+\left[\frac{3}{E-[E_k-2(-1)^j e^{-\theta}/T]}\right]_{T_1}+\cdots,$$
$$k \bmod 4=3 . \quad (4.10d)$$

The reader may verify that Eqs. (4.10c) and (4.10d) describe the fourfold clusters of indices 2 and 3, respectively. We may conclude that the cluster with mean energy E_k has index (k mod4). Since the largest EBK energy is given by $S(E_j)=2\pi j$, the cluster with highest energy has index (j mod4), and we recover the rule of Eq. (3.7).

To summarize, Eq. (4.9) describes the fine and superfine structure of the fourfold clusters, and reproduces the patterns and periodicities in their irrep labels. Apart from the quantization condition Eq. (4.1), our results agree with those of Harter and Patterson. For a comparison between semiclassical and quantum eigenvalues, the reader should consult their papers.[25] For $j=30$, the semiclassically determined fine-structure levels are accurate to within 1%, and the accuracy improves with increasing j. Semiclassical superfine splittings agree with quantum values to within about 5%. It is interesting to note that Harter and Patterson obtain the sign of the superfine splittings, $(-1)^i$, from an analysis of the Wigner 3-j symbols.[24] In our treatment, the sign factor emerges from Maslov phase shifts.

B. Case $E < E_s$

The complex periodic orbit sum for energies less than the classical separatrix energy E_s is carried out in much the same way as the calculation for energies greater than E_s. The presentation in this section is condensed; we point out details which differ from the previous case, and summarize the results.

For energies $E < E_s$, the complex energy shell is topologically equivalent to the spherical lattice shown in Fig. 5(b). The lattice has eight rings, which correspond to the threefold periodic orbits discussed in Sec. III A and shown in Fig. 3(b). These are the primitive periodic orbits of the complex energy shell. We obtain the 24 nodes of the lattice, three to an orbit, by applying the octahedral rotations to the node A, shown in Fig. 5(b). A will be the base point of the complex periodic orbits. The classical segments are one-third cycles of the threefold orbits, with nodes as endpoints. An example is the path from A to C, shown in Fig. 5(b). Each orbit is joined to its three nearest neighbors by tunneling segments, an example of which is the path from A to B. There are two topologically distinct tunneling segments between each pair of neighboring orbits, whose actions differ by a sign. Only one is shown in Fig. 5(b).

As in the preceding calculation, we sum over paths on the lattice which being at A, pass from node to node along classical and tunneling segments, and then return to A. Classical segments must be traversed in the counterclockwise sense, and tunneling must occur along the tunneling segment for which the action is positive imaginary. We adopt the path parametrization of Eq. (2.4). The total phase of the parametrized paths, including the action and Maslov index, is given by

$$\left[\Gamma-\mu\frac{\pi}{2}\right]\{n;a_0,b_1,\ldots,a_n,b_{n+1}\}=\frac{S}{3}\sum_{k=0}^{n}a_k+[i\theta+(j+\tfrac{1}{2})\pi]\sum_{k=1}^{n+1}b_k ,$$

[Eq. (A4) in the Appendix], where S is the action taken around a threefold orbit, and $i\theta$ is the action taken along a tunneling path chosen so that θ is positive. As is explained in the Appendix, the axis of quantization is taken through a fixed point of minimum energy.

We have still to identify the periodic orbits from among the parametrized paths. As in the preceding case, the classical and tunneling segments may be generated by octahedral rotations. It is straightforward to show that the path $\{n;a_0,b_1,\ldots,a_n,b_{n+1}\}$ terminates at the node obtained by applying $\omega^{a_0}\tau^{b_1}\cdots\omega^{a_n}\tau^{b_{n+1}}$ to A, where ω and τ are given by

$$\omega=R_z(\pi/2)R_x(\pi/2) , \quad (4.11a)$$

$$\tau=R_z(\pi/2)R_x(\pi) . \quad (4.11b)$$

[By examining Fig. 5(b), the reader can verify that ω generates the classical segment from the base point A to C, and τ generates the tunneling segment from A to B.] Thus, the path $\{n;a_0,b_1,\ldots,a_n,b_{n+1}\}$ is periodic if and only if the group element $\omega^{a_0}\tau^{b_1}\cdots\omega^{a_n}\tau^{b_{n+1}}=I$. To guarantee that only periodic orbits contribute to the com-

plex periodic orbit sum, we multiply the contribution of each path by the δ function of Eq. (4.4), with ω and τ given by Eq. (4.11).

Substituting Eq. (A3) for the actions and Maslov indices into Eq. (2.3), summing over the parametrized paths of Eq. (2.4), and introducing the coefficients of Eq. (4.4), we obtain the complex periodic orbit sum for energies less than E_s,

$$g_{\rm sc}(E)=\frac{8T}{i}\sum_{n=0}^{\infty}\sum_{a_0=0}^{\infty}\sum_{a_1,\ldots,a_n=1}^{\infty}\sum_{b_1,\ldots,b_n=1}^{\infty}\sum_{b_{n+1}=0}^{\infty}\tfrac{1}{24}\sum_m d_m\chi_m(\omega^{a_0}\tau^{b_1}\cdots\omega^{a_n}\tau^{b_{n+1}})$$
$$\times\exp\left[(iS/3)\sum_k a_k-[\theta-i(j+\tfrac{1}{2})\pi]\sum_k b_k\right]. \tag{4.12}$$

The number of primitive periodic orbits, f in Eq. (2.3), is equal to eight. As in Sec. IV A, we express the characters in terms of the irreducible matrix representatives, and sum the geometric series in the parameters a_k, b_k, and n. We obtain

$$g_{\rm sc}(E)=\frac{T}{3i}\sum_m d_m\,{\rm Tr}\{[\underline{I}_m-e^{iS/3}\underline{D}_m(\omega)-i(-1)^j e^{-\theta}\underline{D}_m(\tau)]^{-1}\}\ . \tag{4.13}$$

To determine the poles of $g_{\rm sc}(E)$, we substitute into Eq. (4.13) explicit matrix representatives for $\underline{D}_m(\omega)$ and $\underline{D}_m(\tau)$, where ω and τ are given by Eq. (4.11). These matrices are given in Ref. 34. Finally, we expand $g_{\rm sc}(E)$ about the EBK energies, sum over the EBK quantum number k, and obtain, to first order in the tunneling amplitude,

$$g_{\rm sc}(E)=\sum_k\left[\left[\frac{1}{(1-r^k)C+r^k(E-E_k)+3(-1)^j e^{-\theta}/T}\right]_{A_1}+\left[\frac{1}{(1-r^k)C+r^k(E-E_k)-3(-1)^j e^{-\theta}/T}\right]_{A_2}\right.$$
$$+\left[\frac{2(2+r^k)}{(1+r^k+r^{2k})C-(r^k+2r^{2k})(E-E_k)}\right]_{E}+\left[\frac{3}{E-E_k-(1-r^k-r^{2k})(-1)^j e^{-\theta}/T}\right]_{T_1}$$
$$\left.+\left[\frac{3}{E-E_k+(1-r^k-r^{2k})(-1)^j e^{-\theta}/T}\right]_{T_2}\right],$$

where

$$r=e^{2\pi i/3}\ \text{and}\ C=\frac{3i}{T}\ . \tag{4.14}$$

Equation (4.14) is our final result for the trace of the energy-dependent Green's function $g_{\rm sc}(E)$ at energies E below the classical separatrix energy E_s. As in Eq. (4.9), we have explicitly identified the terms from the sum over irreps of the octahedral group. According to Eq. (4.14), $g_{\rm sc}(E)$ has poles near the EBK energies E_k. The pole structure depends on the value of (k mod3); the singular terms are those in which the coefficient of C vanishes. It is straightforward to determine the pole structure of $g_{\rm sc}(E)$ for the different cases,[34] as we did in Eq. (4.10). One can verify that Eq. (4.14) reproduces the fine and superfine structure of the threefold clusters in Fig. 4(b), including the symmetry assignments, and correctly determines the index of the cluster with lowest energy, Eq. (3.8). The results agree with those of Harter and Patterson.

C. Symmetry labels

A surprising result of the complex periodic orbit sum is the determination of the eigenvalue symmetry labels. We had no reason to expect this information from the complex periodic orbit prescription, Eq. (2.3). The symmetry labels emerged from the sum over irreducible representations, Eq. (4.4). Recall that this sum was introduced to pick out the contributions of the periodic orbits. In principle, this sum should have been carried out first. However, in deriving Eqs. (4.9) and (4.14), we have interchanged the sum over irreps and the sum over paths. Thus, the poles of Eqs. (4.9) and (4.15) contain contributions from all of the parametrized paths, and not just the periodic orbits. The "unperiodic" orbits appeared at first to be artifacts of the calculation. Now it appears that they contribute to the poles of definite symmetry in an essential way. We have not yet found an explanation of this result. What follows is an interpretation, which may lead to a better understanding of it.

Throughout the calculations we have emphasized the octahedral symmetry of the classical rotational dynamics of SF_6. This symmetry may be exploited as one would a continuous symmetry. By identifying points of the spherical phase space related by symmetry, one may construct a reduced phase space. Note that for continuous symmetries, the reduced phase space has a lower dimension than the original one, while for discrete symmetries, it has the same dimension but a smaller volume. For the present case, the reduced phase space is the wedge-shaped region illustrated in Fig. 6; its area is $\frac{1}{24}$ that of the sphere. A point p on the sphere $|\mathbf{J}|=J$ may be associated with the pair $(\pi(p),g(p))$, where $\pi(p)$ is the point in the reduced phase space related to p by symmetry, and $g(p)$ is the octahedral rotation which maps $\pi(p)$ into p. $g(p)$ plays the role of an ignorable coordinate. One may solve for the dynamics of the reduced phase space, and obtain the evolution of the (discrete) ignorable coordinate by quadrature.

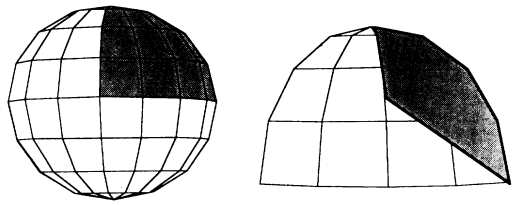

FIG. 6. Symmetry-reduced phase space. (a) Each point on the sphere is equivalent, under fourfold rotations, to a point in the shaded octant. (b) By a threefold rotation, each point in the octant may be mapped into the shaded wedge.

The parametrized paths in the complex periodic orbit sum begin and end at nodes, which are related by symmetry. Therefore, the projection of a parametrized path onto the reduced phase space is a periodic orbit on the reduced phase space. The group element $\omega^{a_0}\tau^{b_1}\cdots\omega^{a_n}\tau^{b_{n+1}}$ represents the value of the ignorable coordinate at the end of this path. Thus, the complex periodic orbit sums of Eqs. (4.5) and (4.14) may be interpreted in the following way. The sums are taken over complex periodic orbits on the reduced phase space. The contribution of each orbit is weighted by the character of the irreducible representation, χ_m, evaluated at the value of the ignorable coordinate at the end of the orbit. The character determines the symmetry of the energy levels; orbits weighted by χ_m produce poles with symmetry m. This interpretation applies to the double well calculation as well. The characters of the cyclic group C_2 produces the poles of definite parity.

The role of symmetry in the periodic orbit sum needs further study. Perhaps the interpretation described here can be extended to continuous symmetries, and may lead to an interesting perspective on the emergence of quantum-mechanical symmetries from semiclassical approximations.

V. CONCLUSION

The rotational spectrum of the SF_6 molecule may be approximately obtained from a sum over classical periodic orbits. The fine structure of the spectrum is generated by the real, or classically allowed orbits, while complex, or classically forbidden orbits produce the superfine structure. Most remarkably, the periodic orbit sum describes the patterns and periodicities in the eigenvalue symmetry assignments. The calculation has also been carried out for the case of half-integral angular momentum.[34] In this case, it is necessary to add to the periodic orbit sum the contributions of orbits which make an even number of revolutions, and subtract the contributions of orbits which make an odd number of revolutions. To distinguish between the two kinds of orbits, we introduce the double octahedral group in Eqs. (4.5) and (4.14).

We have pointed out several heuristic elements of the periodic orbit calculation. These can be divided roughly into two categories. The first concerns the WKB approximation on the spherical phase space, for which a systematic analysis is lacking. The problem is an interesting one; as the classical phase space is compact, the corresponding quantum-mechanical Hilbert space is finite dimensional. The Schrödinger equation on this space is not a differential equation, but rather a difference equation. Various subtleties of the semiclassical treatment, such as the correspondence between quantum operators and classical variables, the Maslov index, and the transmission and reflection coefficients for classically forbidden processes, all need to be developed systematically for the spherical phase space. Recent progress on a related problem has been made by Delos, Waterland, and Du,[35] who have applied the methods of Maslov and Fedoriuk.[36]

The second category of questions concerns the complex periodic orbit sum itself. Given its success, both for the double well and the SF_6 Hamiltonian, it should admit a formal and perhaps a rigorous derivation. Such a derivation has been extensively pursued by Balian, Parisi, and Voros for the case of the quartic oscillator.[9,10] We hope to apply their results to the present work. The representation independence of the periodic orbit theory and its topological flavor make it an appealing method to describe tunneling processes. One motivation underlying Miller's calculation was the hope that complex periodic orbit sums might lead to a description of tunneling in multidimensional systems,[8] for which a complete theory is lacking.[37] We believe this remains a worthwhile goal.

ACKNOWLEDGMENTS

The authors are grateful for the hospitality of the Center for Nonlinear Studies at the Los Alamos National Laboratory. We also thank Dr. Frank K. Molzahn for a careful reading of the manuscript. This work was supported by the U.S. Department of Energy under Contract Nos. DE-AC03-76SF00098 and W7405/ENG-36, and by the National Science Foundation under Grant No. NSF-PYI-84-51276.

APPENDIX

In this appendix we compute the actions and Maslov indices of the parametrized paths of Eq. (2.4) for the SF_6 rotational dynamics. Only the case $E > E_s$ is considered in detail, in Secs. A 1 and A 2. The results for the case $E < E_s$ are quoted in Sec. A 3.

1. The action, $E > E_s$

The action of a parametrized path is the sum of the actions along its segments. Consider the classical segments first. For energies greater than the separatrix energy E_s, the action along a classical segment is one-fourth of the action of the primitive orbit on which it lies; this follows from the fourfold symmetry of the primitive periodic orbits. However, the primitive periodic orbits do not all have the same action. This fact might seem surprising, since these orbits are related by symmetry. The source of the difference is the singularity in the angle ϕ at the north and south poles of the sphere $|\mathbf{J}| = J$. Orbits which enclose either the north or the south pole pick up contributions of $\pm(j+\frac{1}{2})2\pi$ to their actions, the sign depending

on the sense of the orbit. Thus, we need to distinguish between polar orbits, which encircle energy maxima on the $\pm z$ axes, and equatorial orbits, which encircle energy maxima on the $\pm x$ or $\pm y$ axes. If S is the action $\oint dS$ taken around a polar orbit, then the action taken around an equatorial orbit is $S-(j+\frac{1}{2})2\pi$. A polar classical segment (which lies on a polar orbit) has action $S/4$, while an equatorial classical segment (which lies on an equatorial orbit) has action $S/4-(j+\frac{1}{2})\pi/2$. The tunneling segments pose no further complications; they can be chosen so as to have the same action which we take to be $i\theta$, with θ real and positive. Thus, the action of the path $\{n;a_0,b_1,\ldots,a_n,b_{n+1}\}$ is given by

$$\Gamma\{n;a_0,b_1,\ldots,a_n,b_{n+1}\} = \frac{S}{4}\sum_{k=0}^{n} a_k + i\theta\sum_{k=1}^{n+1} b_k - (j+\tfrac{1}{2})\frac{\pi}{2}a_E \ , \quad \text{(A1)}$$

where a_E denotes the number of equatorial calssical segments. It would be difficult to calculate a_E explicitly in terms of the a_k and b_k, but it turns out that it will not be necessary to do so. The difference in the actions of the polar and equatorial classical segments is compensated by a difference in their Maslov indices.

2. Maslov index, $E > E_s$

There is no systematic theory of the Maslov index for spherical phase spaces, so we must define one by analogy. On a flat phase space, the Maslov index is adjusted at the turning points of the configuration space coordinate q. On the spherical phase space $|\mathbf{J}|=J$, we adjust the Maslov index at the turning points of the coordinate ϕ. For the flat phase space, there is a rule which determines the sign of a turning point's contribution to the Maslov index. Along an orbit and in the neighborhood of a turning point, q is regarded as a function of p. At the turning point, $dq/dp=0$. If dq/dp is negative before the turning point and positive after it, the Maslov index is incremented. If the opposite is true, the Maslov index is decremented. We will apply this rule to the spherical phase space, substituting ϕ for q and $-(j+\frac{1}{2})\cos\theta$ for p. Thus, if $d\phi/d(-\cos\theta)$ is negative before a turning point and positive after it, the Maslov index is incremented. Otherwise, it is decremented.

We consider the classical segments first. Along polar classical segments, ϕ is either monotonically increasing or decreasing, and there are no turning points. However, ϕ does have turning points along equatorial classical segments; the turning points coincide with the nodes of the equator. [See, for example, nodes D and E in Fig. 5(a).] As Fig. 5(a) illustrates, before the turning points, ϕ is increasing while $\cos\theta$ is decreasing. That is, $d\phi/d(-\cos\theta)$ is positive. After the turning points, ϕ is decreasing while $\cos\theta$ is decreasing. According the rule obtained above, the Maslov index is decremented.

Using symmetry arguments, we may determine the magnitude of the Maslov index increments. There is no intrinsic difference between polar orbits and equatorial orbits; the distinction arises from our choice of coordinates. Let us demand that both kinds of orbits make identical contributions to the complex periodic orbit sum. From Eq. (2.3), the total phase associated with an orbit is $\Gamma-\mu(\pi/2)$, where Γ is the action of the orbit and μ is its Maslov index. The action of a polar orbit is S, and as we noted above, the action of an equatorial orbit is $S-(j+\frac{1}{2})2\pi$. A polar orbit has no turning points, so its total phase is S. An equatorial orbit has two turning points at which the Maslov index is decremented; its total phase is $S-(j+\frac{1}{2})2\pi+2\mu_0\pi/2$, where μ_0 is the magnitude of the decrement. Requiring the total phases of the orbits to be equal, we find that $S=S-(j+\frac{1}{2})2\pi+2\mu_0\pi/2$. We conclude that $\mu_0=2j+1$. An equatorial orbit consists of four equatorial segments, each of which either begins or ends at a turning point. We divide the Maslov decrements equally among the four equatorial segments, and assign to each a decrement of $j+\frac{1}{2}$.

We consider next the tunneling segments, and in particular, the equatorial tunneling segments, which join two equatorial orbits. An example is the path from D to E in Fig. 5(a). Like the tunneling segments of the double well, the equatorial tunneling segments begin and end at turning points. Since the Maslov index should not be adjusted when an orbit tunnels through a turning point (instead of reflecting from it), we increment the Maslov index by $2j+1$ for each equatorial tunneling segment along a path. What about polar tunneling segments, which join polar orbits to equatorial orbits? These also contribute to the Maslov index because they introduce new turning points. To see this, refer to Fig. 5(a) and consider the polar tunneling segment from the base point A to the node immediately below, B. Along the classical segment leading to A, ϕ is decreasing. Along the classical segment going from B, ϕ is increasing. Thus, ϕ has a turning point along the polar tunneling segment from A to B. According to the sign rule, the Maslov index should be incremented at this turning point. [One can show that $d\phi/d(-\cos\theta)$ is negative before the tunneling segment and positive after it.] Thus, we increment the Maslov index by $2j+1$ at both polar and equatorial tunneling segments.

Collecting the preceding results, we obtain the following formula for the Maslov indices of the parametrized paths:

$$\mu\{n;a_0,b_1,\ldots,a_n,b_{n+1}\} = -(j+\tfrac{1}{2})a_E + (2j+1)\sum_{k=1}^{n+1} b_k \ , \quad \text{(A2)}$$

where a_E denotes the number of equatorial classical segments. Let us combine Eqs. (A1) and (A2) and obtain an expression for the total phase of the parametrized paths,

$$\left[\Gamma-\frac{\pi}{2}\mu\right]\{n;a_0,b_1,\ldots,a_n,b_{n+1}\} = \frac{S}{4}\sum_{k=0}^{n} a_k + [i\theta-(j+\tfrac{1}{2})\pi]\sum_{k=1}^{n+1} b_k \ . \quad \text{(A3)}$$

As is evident from Eq. (4.3), the phase depends only on

the total number of classical and tunneling segments, and not on the number of equatorial segments.

3. Total phase, $E < E_s$

Using arguments analogous to those preceding Eqs. (A1)–(A3), we may determine the actions and Maslov indices of the parametrized paths with energies less than the separatrix energy E_s. It is convenient to choose a new axis of quantization $\bar{z}$, which passes through a fixed point of minimum energy. (In Secs. A 1 and A 2, the axis of quantization was taken to be the z axis, which passes through a fixed point of maximum energy.) The action differential dS is then given by $-J_{\bar{z}}d\bar{\phi}$, where $J_{\bar{z}}$ is the component of angular momentum along the quantization axis, and $\bar{\phi}$ is the azimuthal angle about the axis. Let S be the action around a polar orbit, i.e., an orbit which encircles the $\bar{z}$ axis, and let $i\theta$ be the action along a tunneling segment, chosen so that θ is real and positive. Then the total phase of the parametrized paths is given by

$$\left[\Gamma-\mu\frac{\pi}{2}\right]\{n;a_0,b_1,\ldots,a_n,b_{n+1}\} = \frac{S}{3}\sum_{k=0}^{n}a_k+[i\theta+(j+\tfrac{1}{2})\pi]\sum_{k=1}^{n+1}b_k\ . \quad \text{(A4)}$$

Note that the Maslov phase associated with tunneling segments is positive, whereas in Eqs. (A2) and (A3), it is negative. The change in sign is due to the counterclockwise sense of the threefold orbits, and is consistent with the rule which determines the sign of the Maslov index.

[1]M. C. Gutzwiller, J. Math. Phys. **8**, 1979 (1967); **10**, 1004 (1969); **11**, 1791 (1970); **12**, 343 (1971).

[2]R. Balian and C. Bloch, Ann. Phys. (N.Y.) **60**, 401 (1970); **64**, 271 (1971); **69**, 76 (1972); **63**, 592 (1971); **85**, 514 (1974).

[3]M. V. Berry, in *Semiclassical Mechanics of Regular and Irregular Motion,* Proceedings of the Les Houches Summer School Session XXXVI, Les Houches, 1981, edited by G. Iooss, R. H. G. Hellman, and R. Stora (North-Holland, Amsterdam, 1983), p. 171; M. V. Berry and M. Tabor, Proc. R. Soc. London, Ser. A **349**, 101 (1976); J. Phys. A **10**, 373 (1977).

[4]M. C. Gutzwiller, Phys. Rev. Lett. **45**, 150 (1980); Physica **5D**, 183 (1982).

[5]N. L. Balazs and A. Voros, Phys. Rep. **143**, 109 (1986).

[6]M. L. Du and J. B. Delos, Phys. Rev. Lett. **58**, 1731 (1987).

[7]D. Wintgen, Phys. Rev. Lett. **58**, 1589 (1987); D. Wintgen and H. Friedrich, Phys. Rev. A **35**, 1464 (1987).

[8]W. H. Miller, J. Phys. Chem. **83**, 960 (1979).

[9]R. Balian, G. Parisi, and A. Voros, in *Feynman Path Integrals,* Vol. 106 of *Lecture Notes in Physics,* edited by S. Alberverio (Springer-Verlag, New York, 1979), p. 337.

[10]A. Voros, Ann. Inst. Henri Poincaré **39**, 211 (1983).

[11]D. M. Brink and U. Smilansky, Nucl. Phys. A **405**, 301 (1983).

[12]B. A. Anderson, Ph.D. dissertation, University of Texas at Austin, 1986.

[13]I. Percival, Adv. Chem. Phys. **36**, 1 (1977).

[14]C. W. Patterson, R. S. McDowell, N. G. Nereson, B. J. Krohn, J. S. Wells, and F. R. Peterson, J. Mol. Spectrosc. **91**, 416 (1982).

[15]K. C. Kim, W. B. Person, D. Seitz, and B. J. Krohn, J. Mol. Spectrosc. **76**, 322 (1979).

[16]A. S. Pine and A. G. Robiette, J. Mol. Spectrosc. **80**, 388 (1980).

[17]J. Bordé, Ch. J. Bordé, C. Salomon, A. Van Lerberghe, M. Ouhayoun, and C. D. Cantrell, Phys. Rev. Lett. **45**, 14 (1980).

[18]J. Bordé and Ch. J. Bordé, Chem. Phys. **71**, 417 (1982).

[19]K. T. Hecht, J. Mol. Spectrosc. **5**, 355 (1960).

[20]A. J. Dorney and J. K. G. Watson, J. Mol. Spectrosc. **42**, 135 (1972).

[21]K. Fox, H. W. Galbraith, B. J. Krohn, and J. D. Louck, Phys. Rev. A **15**, 1363 (1977).

[22]W. G. Harter and C. W. Patterson, Phys. Rev. Lett. **38**, 224 (1977).

[23]W. G. Harter and C. W. Patterson, J. Chem. Phys. **66**, 4872 (1977).

[24]C. W. Patterson and W. G. Harter, J. Chem. Phys. **66**, 4886 (1977).

[25]W. G. Harter and C. W. Patterson, J. Chem. Phys. **80**, 4241 (1984).

[26]M. V. Berry and K. E. Mount, Rep. Prog. Phys. **35**, 389 (1972).

[27]N. Fröman and P. O. Fröman, *JWKB Approximation* (North-Holland, Amsterdam, 1965); J. Heading, *Phase Integral Methods* (Methuen, London, 1962).

[28]L. C. Biendenharn and J. D. Louck, in *Encyclopedia of Mathematics and its Applications,* edited by G. Rota (Addison-Wesley, Reading, MA, 1981), Vol. 8.

[29]W. G. Harter, C. W. Patterson, and Fernando J. da Paixao, Rev. Mod. Phys. **50**, 37 (1978).

[30]W. G. Harter, in *Proceedings of the XV Colloquium of Group Theoretical Methods in Physics,* edited by R. Gilmore (World Scientific, Singapore, 1987), p. 1.

[31]C. W. Patterson, B. J. Krohn, and A. S. Pine, J. Mol. Spectrosc. **88**, 133 (1981).

[32]C. W. Patterson, F. Herlemont, M. Azizi, and J. Lemaire, J. Mol. Spectrosc. **108**, 31 (1984).

[33]M. Hamermesh, *Group Theory and its Applications to Physical Problems* (Addison-Wesley, Reading, MA, 1962), p. 107.

[34]J. M. Robbins, Ph.D. thesis, University of California, Berkeley, 1989.

[35]J. B. Delos, R. L. Waterland, and M. L. Du, Phys. Rev. A **37**, 1185 (1988).

[36]V. P. Maslov and M. V. Fedoriuk, *Semiclassical Approximation in Quantum Mechanics* (Reidel, Boston, 1981).

[37]M. Wilkinson, Physica **21D**, 341 (1986).

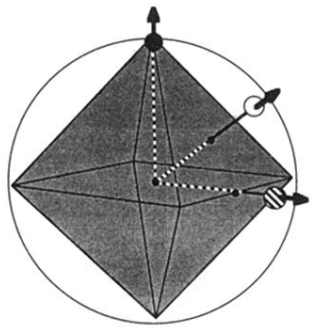

FIG. 2. Fixed points of SF_6 Hamiltonian. An octahedron is inscribed in the sphere of constant angular momentum. Energy maxima lie along axes through the vertices of the octahedron, saddle points along axes through the faces, and energy minima along axes through the edges of the octahedron. Only one of each type of fixed point is shown.

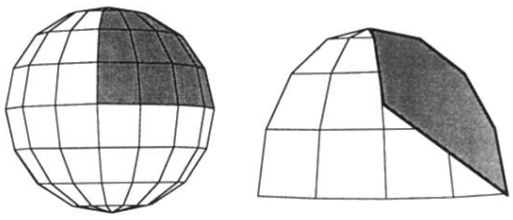

FIG. 6. Symmetry-reduced phase space. (a) Each point on the sphere is equivalent, under fourfold rotations, to a point in the shaded octant. (b) By a threefold rotation, each point in the octant may be mapped into the shaded wedge.